J|A|C|S ARTICLES

Published on Web 10/06/2009

Surface and Bulk Aspects of Mixed Oxide Catalytic Nanoparticles: Oxidation and Dehydration of CH_3OH by Polyoxometallates

Lingaiah Nakka,† Julie E. Molinari, and Israel E. Wachs*

Operando Molecular Spectroscopy & Catalysis Laboratory, Chemical Engineering Department, Lehigh University, Bethlehem, Pennsylvania 18015

Received June 18, 2009; E-mail: iew0@lehigh.edu

Abstract: The molecular structures and surface chemistry of mixed metal oxide heteropolyoxo vanadium tungstate ($H_{3+x}PW_{12-x}V_xO_{40}$ with $x = 0$, 1, 2, and 3) Keggin nanoparticles (NPs), where vanadium is incorporated into the primary Keggin structure, and supported VO_x on tungstophosphoric acid (TPA, $H_3PW_{12}O_{40}$), where vanadium is present on the surface of the Keggin unit, were investigated with solid-state magic angle spinning ^{51}V NMR, FT-IR, in situ Raman, in situ UV−vis, CH_3OH temperature-programmed surface reaction (TPSR), and steady-state methanol oxidation. The incorporated VO_x unit possesses one terminal V═O bond, four bridging V−O−W/V bonds, and one long V−O−P bond in the primary Keggin structure, and the supported VO_x unit possesses a similar coordination in the secondary structure under ambient conditions. The specific redox reaction rate for VO_x in the Keggin primary structure is comparable to that of bulk V_2O_5 and the more active supported vanadium oxide catalysts. The specific acidic reaction rate for the WO_x in the TPA Keggin, however, is orders of magnitude greater than found for bulk WO_3, supported tungsten oxide catalysts, and even the highly acidic WO_3−ZrO_2 catalyst synthesized by coprecipitation of ammonium metatungstate and $ZrO(OH)_2$. From CH_3OH-TPSR and in situ Raman spectroscopy it was found that incorporation of vanadium oxide into the primary Keggin structure is also accompanied by the formation of surface VO_x species at secondary sites on the Keggin outer surface. Both CH_3OH-TPSR and steady-state methanol oxidation studies demonstrated that the surface VO_x species on the Keggin outer surface are significantly less active than the VO_x species incorporated into the primary Keggin structure. The presence of the less active surface VO_x sites in the Keggins, thus, decreases the specific reaction rates for both methanol oxidation and methanol dehydration. During methanol oxidation/dehydration ($O_2/CH_3OH = 2.17$, $T = 225$ °C), in situ UV−vis diffuse reflectance spectroscopy revealed that vanadium oxide is primarily present as the V^{+5} cation, which reflects the Mars−van Krevelen redox mechanism and rapid reoxidation by molecular O_2. The bulk TPA Keggin structure becomes more disordered and less thermally stable as the vanadium content increases. Although surface polyaromatic carbon forms during methanol oxidation on the Keggin surfaces, its influence on the reaction kinetics seems minimal as the carbon content diminishes as the vanadium oxide content increases and the reaction temperature is raised. No relationships were found between the electronic structure (UV−vis E_g values) and TOF_{redox} and TOF_{acid} (TOF = turnover frequency) kinetics, which reflect the complexity of $H_{3+x}PW_{12-x}V_xO_{40}$ Keggins. The overall catalytic performance of the $H_{3+x}PW_{12-x}V_xO_{40}$ Keggin materials results from a complex interplay among the presence of redox vanadium (as secondary surface VO_x species and substituted VO_x sites in the primary Keggin NP structure), structural disorder of the Keggin NPs, exposed surface acid and redox sites, and coke deposition. These new insights reveal that the Keggin heteropolyoxometallates are much more complex than originally thought and that care must be taken in using Keggins as model mixed metal oxide NPs in catalytic kinetic and theoretical studies because their surface and bulk structures are dynamic under the reaction conditions.

Introduction

Polyoxometallates (POMs) are viewed as ideal subnanometer mixed oxide particles possessing a dimension of ∼0.8 nm.[1] The POM Keggin cluster consists of a central cation (e.g., P, Si, Ti, etc.) that is surrounded by 12 metal oxide cations (e.g., W, Mo, etc.).[2] Each metal oxide cation possesses one terminal M═O bond, four bridging M−O−M bonds, and one long M−O−P bond. The negatively charged mixed metal oxide POM cluster is charge balanced by surface protons. The molecular structural chemistry of POM catalysts can be tuned by the substitution of different cations or by exchanging the POM surface protons with surface cations.[3] For example, one or more of the primary

† Permanent address: Catalysis Laboratory, I&PC Division, Indian Institute of Chemical Technology, Hyderabad-500607, India.

(1) Pope, M. T.; Muller, A. *Angew. Chem., Int. Ed. Engl.* **1991**, *30*, 34.

(2) Tsigdinos, G. A. *Top. Curr. Chem.* **1978**, *76*, 1.

(3) Mizuno, N.; Hann, W.; Kudo, T. *J. Catal.* **1998**, *178*, 391.

10.1021/ja904957d CCC: $40.75

W^{6+} cations in the $H_3PW_{12}O_{40}\cdot nH_2O$ Keggin structure can be substituted by V^{5+} cations, and the charge imbalance is compensated by additional surface protons or even surface inorganic cations in the surrounding secondary structure.[4,5]

Keggin clusters have generated much interest as catalysts since their constitutional elements can readily be varied and tuned for acidic and redox catalytic applications.[6−8] For example, vanadium oxide addition to the acidic $H_3PW_{12}O_{40}\cdot nH_2O$ Keggin enhances its catalytic partial oxidation properties because vanadia introduces redox character to the $H_{3+x}PW_{12-x}V_xO_{40}\cdot nH_2O$ POM.[9] Vanadium-containing $H_{3+x}PMo_{12-x}V_xO_{40}\cdot nH_2O$ POMs have been investigated as mixed metal oxide catalysts for partial oxidation of alcohols and alkanes.[10−12] The ability of mixed metal oxide POMs to perform selective oxidation reactions has stimulated much interest in this class of catalytic materials and motivated a deeper fundamental understanding of their molecular structural chemistry and its relationship to their catalytic performance. The establishment of molecular structure−catalytic performance relationships is made all the more challenging because it has been shown that the structure of the POM catalysts can change under the reaction conditions and may not necessarily correspond to the ideal crystallographic structure of the originally prepared Keggin-type material.[13,14] Thus, in situ molecular structural characterization of mixed metal oxide POMs under different environmental conditions must be collected to be able to establish their fundamental molecular structure−activity relationships.[15] In addition to the bulk structures of POMs in reactive environments, there currently is no information about the surface composition of POMs under partial oxidation/dehydration reaction conditions.

The objective of this investigation is to examine both the surface and bulk properties of the subnanometer-sized Keggin POMs during the partial oxidation/dehydration of CH_3OH over $H_{3+x}PW_{12-x}V_xO_{40}\cdot nH_2O$ mixed metal oxide Keggins, where it will be converted to HCHO over surface redox sites and to CH_3OCH_3 (DME, dimethyl ether) over surface acid sites, to determine their molecular structure−performance relationships. Unlike the more investigated molybdenum-based POMs ($H_{3+x}PMo_{12-x}V_xO_{40}$),[10−12] the tungsten-containing POMs have not received much attention as partial oxidation catalysts because of their stronger acidic character.[16] In the present investigation, the vanadium-containing $H_{3+x}PW_{12-x}V_xO_{40}$ ($x = 0$, 1, 2, and 3) will be examined for the influence of vanadia upon the Keggin surface composition, bulk structure, and surface reactivity during methanol oxidation/dehydration. The surface chemistry and composition of the V-containing tungstophosphoric acid (TPA) Keggins will be chemically probed by CH_3OH temperature-programmed surface reaction (TPSR) spectroscopy and steady-state methanol oxidation. In situ Raman spectroscopy will be employed to determine the surface and bulk Keggin molecular structural chemistry during methanol oxidation. In situ UV−vis will be employed to determine the corresponding electronic structures of the mixed metal oxide POMs. These studies will provide new fundamental insights into the subnanometer-sized mixed metal oxide Keggin POMs.

Experimental Section

Catalysts. The $H_3PW_{12}O_{40}$ and $H_{3+x}PW_{12-x}V_xO_{40}$ ($x = 1$, 2, 3) POMs were purchased from Aldrich Chemical Co. and Nippon Inorganic Color and Chemical Co., respectively. The vanadium-containing tungstophosphoric acid, $H_{3+x}PW_{12-x}V_xO_{40}$ ($x = 1$, 2, 3), catalysts will be denoted by TPAV1, TPAV2, and TPAV3, respectively. In addition, vanadia was also introduced onto the surface or secondary structure of TPA, and this catalyst is denoted as VOTPA.[17] An aqueous solution containing an appropriate amount of VO^{2+} ions was prepared by reaction of crystalline V_2O_5 with oxalic acid at about 100 °C with maintenance of the VO^{2+}/TPA molar ratio equal to 2. After complete dissolution of the V_2O_5 solid, the solution was cooled to room temperature, and the required amount of TPA was added. The excess water was then removed by evaporation at 100 °C, and the dried mass was subsequently calcined at 300 °C in air for 3 h.

Solid-State ^{51}V NMR. Solid-state magic angle spinning (MAS) ^{51}V NMR spectra were recorded under ambient conditions on a General Electric model GN-300 NMR spectrometer at 78.89 MHz. The instrument was equipped with a Nicolet 2090-IIIA high-speed digital oscilloscope and a 5 mm MAS NMR Doty Scientific probe. The measurements were carried out on static samples with a simple one-pulse excitation of 1 μs width, a preacquisition delay of 10 μs, a dwell time of 0.5 μs, and a relaxation delay of 4 s. Prior to Fourier transformation, the signal-averaged free induction decays were multiplied by an exponential function equivalent to 500 Hz line broadening to decrease noise in the spectra. All chemical shifts were referenced against liquid $VOCl_3$.

Raman Spectroscopy. The in situ Raman spectra of the POMs were collected with a Horiba-Jobin Yvon LabRam-HR spectrometer equipped with a confocal microscope, 2400/900 grooves/mm gratings, and a notch filter. The visible laser excitation at 532 nm (visible/green) was supplied by a Yag doubled diode pumped laser (20 mW). The scattered photons were directed and focused onto a single-stage monochromator and measured with a UV-sensitive LN_2-cooled CCD detector (Horiba-Jobin Yvon CCD-3000 V). The powdered samples, ~5−10 mg, were loosely spread onto a small ceramic boat inside the environmental cell (Linkam T-1500) and maintained below the confocal microscope. Dehydration of the catalyst samples was carried out by heating the environmental cell to different temperatures under O_2/He or CH_3OH/O_2/He flow (30 mL/min). After the desired treatment temperature was reached, the samples were dehydrated for 30 min before the Raman spectrum was recorded. The W−O−W bending modes at ~220−250 cm^{-1} were employed as an internal standard to normalize the intensity of the Raman spectra since these vibrations originate from the intact Keggin unit and are least sensitive to the environmental conditions.

FT-IR Spectroscopy. The IR spectra were obtained under ambient conditions with a Bio-Rad FTS-40A FT-IR spectrometer equipped with a DTGS detector. The IR spectra were recorded with a resolution of 2 cm^{-1} using 250 signal-averaged scans using the KBr disk method.

UV−Vis Diffuse Reflectance Spectroscopy (DRS). Solid catalyst samples were examined using a Varian Cary 5E UV−vis spectrophotometer equipped with the Harrick Praying Mantis

(4) Okuhara, T.; Mizuno, N.; Misono, M. *Adv. Catal.* **1996**, *41*, 113.
(5) Neumann, R.; Dror, I. *Appl. Catal., A* **1998**, *172*, 67.
(6) Misono, M. *Chem. Commun.* **2001**, 1141.
(7) Mizuno, N.; Misono, M. *Chem. Rev.* **1998**, *98*, 198.
(8) Hill, C. L.; Posser-McCarthy, C. M. *Coord. Chem. Rev.* **1995**, *143*, 407.
(9) Brückman, K.; Tatibouet, J. M.; Che, M.; Serwicka, E.; Haber, J. *J. Catal.* **1993**, *139*, 455.
(10) Liu, H.; Iglesia, E. *J. Phys. Chem. B.* **2003**, *107*, 10840.
(11) Centi, G.; Lena, V.; Trifiro, F.; Ghoussoub, D.; Aissi, C. F.; Guelton, M.; Bonnelle, J. P. *J. Chem. Soc., Faraday Trans.* **1990**, *86*, 2775.
(12) Marchal-Roch, C.; Bayer, R.; Moisan, J. F.; Tezé, A.; Hervé, G. *Top. Catal.* **1996**, *3*, 407.
(13) Watzenberger, O.; Emig, G.; Lynch, D. T. *J. Catal.* **1990**, *124*, 247.
(14) Lee, K. E.; Melsheimer, J.; Berndt, S.; Mestl, G.; Schlögl, R.; Köhler, K. *Appl. Catal., A* **2001**, *214*, 125.
(15) Ressler, T.; Timpe, O.; Girgsdies, F.; Wienold, J.; Neisius, T. *J. Catal.* **2005**, *231*, 279.
(16) Kozhevnikov, I. V. *Chem. Rev.* **1998**, *98*, 171.
(17) Casarini, D.; Centi, G.; Jiru, P.; Lena, V.; Tvaruzkova, Z. *J. Catal.* **1993**, *143*, 325.

attachment (model DRA-2) for diffuse reflectance spectroscopy. The reference laser was passed through a 1.5 absorbance unit filter to minimize background noise. Approximately 30 mg of each finely ground sample was loaded into the cup of the Harrick cell (model HVC-DR2 with a high-pressure dome). A magnesium oxide white reflectance standard baseline was collected under ambient conditions. The spectrum of each catalyst sample was collected over the wavelength range of 200−800 nm under ambient conditions, under dehydrated conditions at 225 °C, and under in situ reaction conditions during methanol oxidation ($O_2/CH_3OH = 2.17$). The UV−vis DRS spectra were analyzed using the Kubelka−Munk function $F(R_¥)$ and evaluated for the band gap value (E_g) using methods described by Gao[18] and Ross-Medgaarden.[19]

CH_3OH-TPSR Spectroscopy. The CH_3OH-TPSR spectroscopy measurements were performed on an Altamira (AMI-200) system equipped with an online quadrupole mass spectrometer (Dycor Dymaxion DME200MS). About 200 mg of sample was typically loaded into a U-shaped quartz tube and initially treated at 250 °C (ultra zero grade O_2/He, 30 mL/min) for ∼1 h to remove any combustible impurities that may be present. To ensure that the catalysts remain in a fully oxidized state, the pretreated samples were first cooled in flowing air to 110 °C and then the gas stream was switched to an ultra-high-purity He flow with further cooling to 100 °C. After flushing with continuously flowing He for another 1 h at 100 °C to remove any physically adsorbed oxygen or potential background gases, a CH_3OH/He gas mixture (2000 ppm methanol) feed was introduced at 30 mL/min for CH_3OH chemisoprtion and maintained for ∼40 min. Previous work demonstrated that the adsorption temperature of 100 °C almost completely minimizes the presence of physically adsorbed methanol on the catalyst samples since the physically adsorbed CH_3OH desorbs below this temperature.[20] After methanol adsorption, the POM catalysts were again purged at 100 °C with an ultra-high-purity (UHP) He flow for an additional 1 h to remove any residual physically adsorbed methanol. The CH_3OH-TPSR spectroscopy experiment was then performed with a heating rate of 10 °C/min in the flowing UHP He, and the desorption products were monitored with the online mass spectrometer. The *m*/*e* values used to detect the different desorption products were 31 (CH_3OH), 30 (H_2CO), 45 (CH_3OCH_3−DME), 76 ($(CH_3O)_2CH_2$−DMM), 44 (CO_2), and 28 (CO). For desorbing products that gave rise to several fragments in MS, additional *m*/*e* values were also collected to confirm the identity of the desorbing products (e.g., $m/e = 45$ for $CH_3OCH_2^+$ and $m/e = 15$ for the associated CH_3^+ cracking fragment). The number of exposed redox and acid sites per gram (N_s) of each catalyst was determined from the TPSR spectra. The area under the curve for the formaldehyde peak was integrated to determine the number of redox sites, and the area under the curve for the dimethyl ether peak was integrated to determine the number of acid sites. The MS signals for HCHO and DME were calibrated against quantitative thermogravimetric analysis (TGA) measurements with exclusive redox and acid catalysts, respectively.

CH_3OH Oxidation/Dehydration. Steady-state methanol oxidation was performed in an isothermal fixed-bed differential reactor at atmospheric pressure. In a typical experiment about 30 mg of catalysts was held between two glass wool beds and pretreated under O_2/He flow at 250 °C for 30 min before passing the gaseous reactants at the desired reaction temperature. The volume composition of the gaseous reactant feed was 6% CH_3OH, 13% O_2, and balance He, with a total flow rate of ∼100 mL/min. The methanol conversion and reaction products were analyzed using an online gas chromatograph (HP 5890 series II) equipped with TCD and FID detectors. A Carboxene-1000-packed column and a CP-sil 5CB capillary column were used in parallel for TCD and FID, respectively. The catalytic turnover frequencies (TOFs) for methanol oxidation to redox products (HCHO, MF, and DMM) and methanol dehydration to DME were determined by normalizing the steady-state reaction rates per gram by the number of redox and acid sites per gram of catalyst, respectively, which were determined from CH_3OH-TPSR.

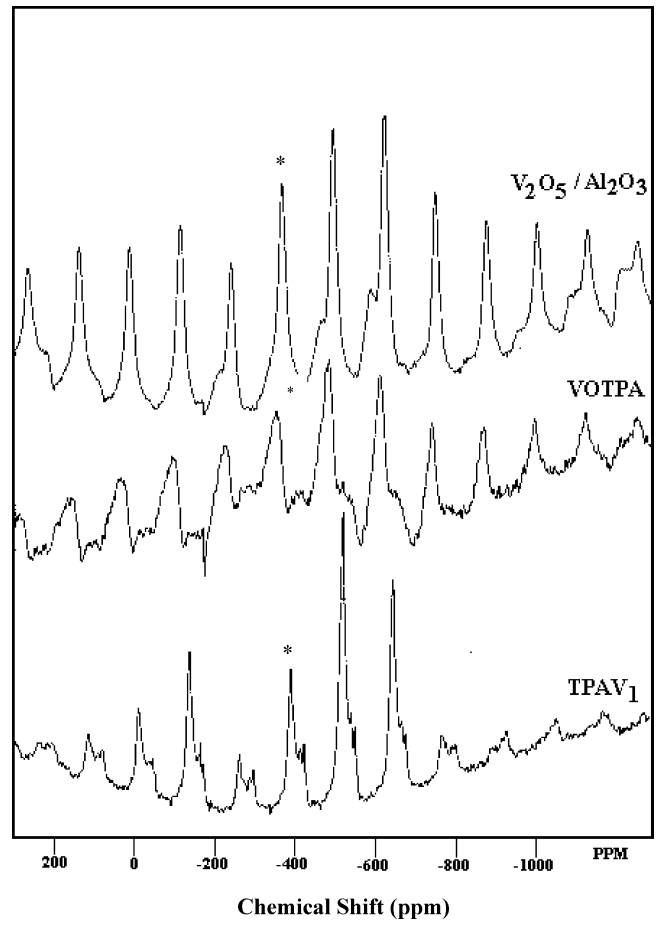

Figure 1. Solid-state MAS ^{51}V NMR spectra of VOTPA and TPAV1 catalysts under ambient conditions (the asterisk indicates the central band).

Results

Solid-State MAS ^{51}V NMR under Ambient Conditions. Solid-state MAS ^{51}V NMR studies were undertaken to determine the local coordination of the VO_x sites in the V-containing TPA mixed oxide Keggins under ambient conditions where the POMs are in a hydrated state from background moisture. The MAS ^{51}V NMR spectra of the catalysts are shown in Figure 1. The solid-state MAS ^{51}V NMR chemical shift for the supported 20% V_2O_5/Al_2O_3 under ambient conditions was taken as a reference since prior NMR studies have demonstrated that only hydrated VO_6 species are present for this sample under ambient conditions.[21] The solid-state MAS ^{51}V NMR chemical shift for supported 20% V_2O_5/Al_2O_3 under ambient conditions exhibits a central band at −362 ppm characteristic of VO_6 sites. The chemical shifts for TPAV1 and VOTPA occur at −385 and −246 ppm, reflecting the VO_6 coordination of the hydrated VO_x sites in these V-containing TPA Keggins. The VO_6 coordination for the VOTPA catalyst is consistent with the VO_6 unit substituting for one of the WO_6 units in the TPA Keggin structure. The VO_6 coordination for the hydrated VOTPA

(18) Gao, X.; Wachs, I. E. *J. Phys. Chem.* **2000**, *104*, 1261.
(19) Ross-Medgaarden, Wachs, I. E. *J. Phys. Chem. C* **2007**, *111*, 15089.
(20) Briand, L. E.; Farneth, W. E.; Wachs, I. E. *Catal. Today* **2000**, *62*, 219.
(21) Eckert, H.; Wachs, I. E. *J. Phys. Chem.* **1989**, *93*, 6796.

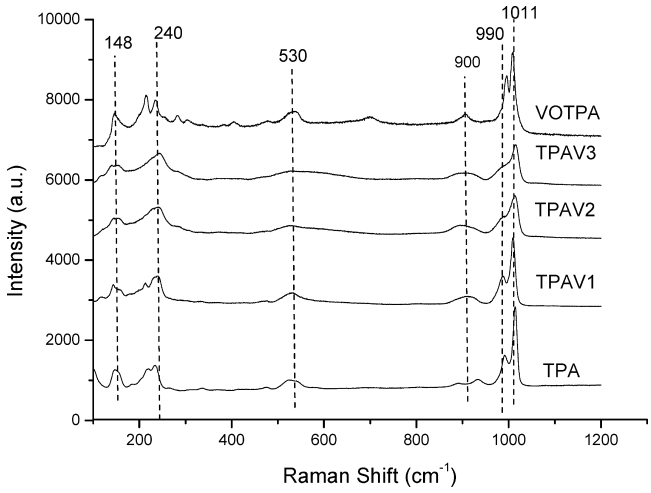

Figure 2. Raman spectra of V-containing tungstophosphoric acid, $H_{3+x}PW_{12-x}V_xO_{40}$ (x = 0, 1, 2, and 3), and VOTPA (supported VO_x/$H_3PW_{12}O_{40}$) polyoxometallates under ambient conditions. The Raman spectra were normalized against Keggin W−O−W bending modes at ~220−250 cm^{-1}.

catalyst is consistent with the very low pH at the PZC of this sample (PZC ≈ 0.5).[22]

Raman and FT-IR Spectroscopy under Ambient Conditions. The Raman spectra of the $H_{3+x}PW_{12-x}V_xO_{40}$ (x = 0, 1, 2, and 3) and VOTPA mixed oxide Keggins under ambient conditions are presented in Figure 2, and their assignments are given in Table 1. The V-free TPA Raman spectrum exhibits strong W═O_t symmetric and asymmetric stretching modes at 1011 and 990 cm^{-1}, respectively. The asymmetric stretch is a consequence of the presence of vibrationally coupled adjacent W═O_t bonds in the Keggin structure. The weaker Raman bands at 890 and 530 cm^{-1} are characteristic of the asymmetric stretching vibration of bridging W−O_b−W (O_b denotes a corner-sharing bridging oxygen atom) and symmetric stretching of bridging W−O_c−W (O_c denotes an edge-sharing bridging oxygen atom), respectively. The Raman band at ~240 cm^{-1} represents the bending mode of the bridging W−O−W bonds of the intact Keggin structure. These Raman spectra agree with those reported in the literature.[23,24] The vanadia-substituted TPA and VOTPA mixed oxides also exhibit Raman bands that are similar to those of the TPA Keggin, but the resolution of the W═O_t vibrations at 1011 and 990 cm^{-1} decreases as the vanadia content is increased. The similar Raman bands for TPA, TPAV, and VOTPA reveal that the Keggin structure remains intact upon incorporation of vanadia into the primary and secondary structures.

The corresponding FT-IR spectrum of tungstophosphoric acid under ambient conditions is presented in Figure 3 and shows bands at 1080, 981, 888, 797, and 595 cm^{-1} that are related to asymmetric vibrations of P−O_a, W═O_t, W−O_b−W, and W−O_c−W and the bending mode of O_a−P−O_a, respectively. The FT-IR band assignments are given in Table 1. The oxygen atom bridging the central P and W atoms, P−O_a−W, is denoted as O_a. Comparison of the Raman and IR bands reveals that IR gives rise to a stronger band than Raman at 1080 cm^{-1} related to the P−O_a asymmetric stretch. The corresponding symmetric P−O_a band vibration is not observed in the Raman spectrum, which is most probably related to its weaker Raman cross section compared to the strong W═O_t vibrations. The P−O_a vibration, however, is not generally observed with Raman spectroscopy for polyoxometallates in the solid form, but such a weak Raman band has been detected for molybdophosphoric acid in aqueous solution.[25] The Raman and IR vibrational assignments are summarized in Table 1.

The supported VOTPA catalyst exhibits the main infrared bands (Figure 3) characteristic of the Keggin anion at 1080 (P−O_a asymmetric), 981 (W═O_t asymmetric), 888 (W−O_b−W asymmetric), and 803 (W−O_c−W asymmetric) cm^{-1}. When vanadium is incorporated into the primary Keggin structure in TPAV1, a shift is observed and the P−O_a band splits (see also Table 2). Such a shift is not observed for the supported VOMPA sample where vanadium is presented in the secondary structure as a surface VO_x species. The TPAV1 catalyst with vanadium in the Keggin primary structure also shows a shoulder band at 1097 cm^{-1}. This infrared band is due to the asymmetric vibration of the P−O_a−V bond.[26] The splitting of the P−O_a band is due to the introduction of a cation other than W into the Keggin structure, which induces a decrease in the W−O_t stretching frequency, leading to splitting of the P−O_a band,[27] thus confirming the incorporation of vanadium into the primary Keggin structure for TPAV1. The incorporation of vanadium into the primary TPA structure leads to a shift and splitting of the main FT-IR band due to the reduced structural symmetry as shown by the vibrational bands listed in Table 2.[17] A clear shift in the P−O_a vibration (O_a denotes an oxygen atom bound to three W atoms and to P) is noticed from 1080 cm^{-1} for TPA to 1069 cm^{-1} for the TPAV3 sample. This shift in the P−O_a band position reflects the incorporation of vanadium into the primary structure of the tungstophosphoric acid Keggin.

In Situ Raman Spectroscopy under Dehydrated Conditions. The in situ Raman spectra of the dehydrated POM Keggins at 200 °C are contained in Figure 4 and are normalized against the TPA Keggin W−O−W bending modes at ~220−250 cm^{-1}. No additional Raman bands from the V═O_t vibrations are observed because of the stronger Raman features of the W═O_t vibrations that are broadened by the presence of VO_x. The dehydrated Raman spectra exhibit a shift of the W═O_t vibration from 1011 to 1022 cm^{-1} due to the loss of crystal water.[28] Such Mo═O_t vibrational shifts upon dehydration have previously been reported for $H_3SiMo_{12}O_{40}$ and are simply related to desorption of water and removal of its associated hydrogen bonding (M═O_t···H−OH).[29] There is no significant shift in the position of all other bands upon dehydration since dehydration primarily affects the terminal W═O_t vibrations.

The addition of the surface VO_x species to the TPA in supported VOTPA results in enhanced Raman bands at ~984 and ~930 cm^{-1} as well as a slight shift of the W═O_t vibration to lower wavenumbers that reflects perturbation of the WO_x vibrations in the primary Keggin structure by the presence of surface VO_x species. The shift from 1022 to 984 cm^{-1} appears

(22) Deo, G.; Wachs, I. E. *J. Phys. Chem.* **1991**, *95*, 5889.
(23) Busca, G. *J. Raman Spectrosc.* **2002**, *33*, 348.
(24) Caliman, E.; Dias, J. A.; Dias, S. C. L.; Prado, A. G. S. *Catal. Today* **2000**, *107−108*, 816.
(25) Mestl, G.; lkenhans, I. T.; Spielbauer, D.; Dieterle, M.; Timpe, O.; Kröhnert, J.; Jentoft, F.; Knözinger, H.; Schlögl, R. *Appl. Catal., A* **2001**, *210*, 13.
(26) Shinach, S.; Matsushita, M.; Yamaguchi, K.; Mizuno, N. *J. Catal.* **2005**, *233*, 81.
(27) Rocchiccioli-Deltcheff, C.; Fournier, M. *J. Chem. Soc., Faraday Trans.* **1991**, *87*, 3913.
(28) Brown, G. M.; Noe-Spirlet, M. R.; Busing, W. R.; Levy, H. A. *Acta Crystallogr.* **1977**, *B33*, 1038.
(29) Banares, M. A.; Hu, H.; Wachs, I. E. *J. Catal.* **1995**, *155*, 249.

Table 1. Comparison of FT-IR and Raman Spectra for Tungsten- and Vanadium-Containing Polyoxometallate Catalysts under Ambient Conditions[a]

	FT-IR		Raman	
sample	band position (cm^{-1})	assignment	band position (cm^{-1})	assignment
$H_3PW_{12}O_{40}$	1080 (s)	$P-O_a$ asymmetric stretch		
			1011 (s)	$W=O_t$ symmetric stretch
	984 (s)	$W=O_t$ asymmetric stretch	990 (m)	$W=O_t$ asymmetric Stretch
			930 (w)	$W-O_b-W$ asymmetric stretch
	888 (s)	$W-O_b-W$ asymmetric stretch	890 (vw)	
	797 (m)	$W-O_c-W$ asymmetric stretch		
	595 (w)	O_a-P-O_a asymmetric bending		
			530	$W-O_c-W$ symmetric stretch
			325 (vw)	W−O bending
			225 (m)	W−O−W bending
			242 (m)	
			148 (w)	lattice phonon
$H_3PW_{11}V_1O_{40}$	1097 (vw)	$(P-O_a-V)$ asymmetric stretch		
	1078 (s)	$P-O_a$ asymmetric stretch		
			1011 (s)	$W=O_t$ symmetric stretch
	981 (s)	$W=O_t$ asymmetric stretch	990 (m)	$W=O_t$ asymmetric stretch
			930 (w)	
	886 (s)	$W-O_b-W$ asymmetric stretch	890 (vw)	$W-O_b-W$ asymmetric stretch
	797 (m)	$W-O_c-W$ asymmetric stretch		
	595 (w)	O_a-P-O_a bending	530 (w)	$W-O_c-W$ symmetric stretch
			325 (vw)	W−O bending
			225 (vw), 242 (m)	W−O−W bending
			148 (w)	lattice phonon

[a] Key: O_a, oxygen atom bound to three W atoms and to P; O_t, terminal oxygen atom; O_b, corner-sharing bridging oxygen atom; O_c, edge-sharing bridging oxygen atom; s, strong; m, medium; w, weak; vw, very weak.

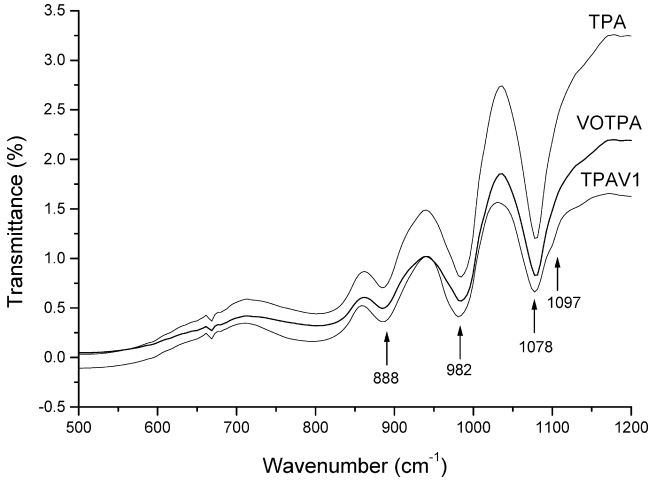

Figure 3. FT-IR spectra of hydrated TPA, VOTPA, and TPAV1 catalysts under ambient conditions.

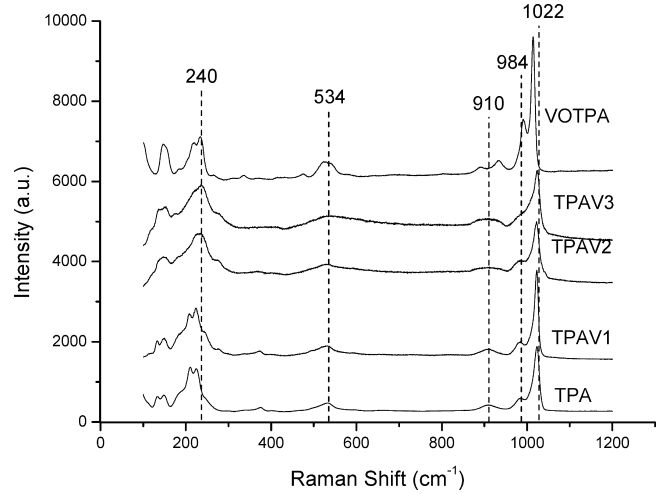

Figure 4. In situ Raman spectra of dehydrated V-containing tungstophosphoric acid, $H_{3+x}PW_{12-x}V_x$ (x = 0, 1, 2, and 3), and VOTPA (supported $VO_x/H_3PW_{12}O_{40}$) polyoxometallates (200 °C). The Raman spectra were normalized against Keggin W−O−W bending modes at ∼220−250 cm^{-1}.

Table 2. Comparison of FT-IR Stretching Frequencies of the Main Characteristic Bands for TPA and Vanadium-Containing Tungstophosphoric Acid (TPAV1, TPAV2, and TPAV3) Catalysts under Ambient Conditions[a]

	IR stretching frequency (cm^{-1})			
sample	$P-O_a$	$W=O_t$	$W-O_b-W$	$W-O_c-W$
TPA	1080	984	890	800
TPAV1	1078	981	886	797
TPAV2	1073	980	881	795
TPAV3	1069	978	876	795

[a] Key: O_a, oxygen atom bound to three W atoms and to P; O_t, terminal oxygen atom; O_b, corner-sharing bridging oxygen atom; O_c, edge-sharing bridging oxygen atom.

to be related to perturbation of the vibrational coupling of adjacent $W=O_t$ bonds since the WO_t vibration for supported tungsten oxide catalysts also shifts from ∼990 to 1020 cm^{-1} as the surface WO_x species become polymerized and the $W=O_t$ bonds become vibrationally coupled.[30] Thus, the new Raman band at ∼984 cm^{-1} is related to the symmetric $W=O_t$ stretch of tungsten oxide interacting with surface VO_x species, and that at ∼930 cm^{-1} is either the associated asymmetric stretch or the perturbed asymmetric W−O−W stretch of the TPA Keggin.

The in situ Raman spectra of TPA, TPAV, and VOTPA POMs as a function of calcination temperature from 300 to 600 °C in flowing O_2/He were also examined (see the Supporting Information, Figures SI-1−SI-5). The Raman spectra of these POMs at 300 °C are similar to their dehydrated spectra at 200 °C shown in Figure 4, with only a small difference in the spectrum of TPAV3, which demonstrates that the POM Keggin

(30) Kim, T.; Wachs, I. E. *J. Catal.* **2008**, *255*, 197.

structures are thermally stable up to ~300 °C. The vanadia-free TPA POM is thermally stable in this temperature range, and the bands thermally broaden as 600 °C is approached. In contrast, the V-containing POMs begin to decompose at temperatures of 400−500 °C. Decomposition of the V-containing Keggin structures is accompanied by the appearance of a small band at ~1034 cm^{-1} that is characteristic of the V=O vibration of the surface VO_x species in the secondary structure[31,32] and is accompanied by broad bands at 690 and 790 cm^{-1} that become sharper with increasing temperature from formation of crystalline WO_3 nanoparticles (NPs).[33] These observations demonstrate that incorporation of vanadia into the TPA primary and secondary structures leads to destabilization of the TPA Keggin during thermal treatments at elevated temperatures. Thus, the presence of surface VO_x species enhances the destabilization of the TPA Keggin at elevated temperatures. All the TPAV and the supported VOPTPA catalysts, however, are thermally stable below 300 °C.

The W=O_t and V=O_t bond lengths in the Keggins were also determined from established W−O and V−O bond length−vibration diatomic correlations.[28,31,34] The symmetric W=O_t vibration occurs at ~1022 cm^{-1} for the dehydrated $H_3PW_{12}O_{40}$, $H_{3+x}PW_{12-x}V_xO_{40}$, and supported $VO_x/H_3PW_{12}O_{40}$ catalysts. The vibration at 1022 cm^{-1} corresponds to a W=O_t bond length of 0.1698 nm, and the vibration at 534 cm^{-1} corresponds to a bond length of 0.2039 nm. The symmetric V=O_t vibration for the dehydrated $H_{3+x}PW_{12-x}V_xO_{40}$ and supported $VO_x/H_3PW_{12}O_{40}$ catalysts is not detectable because it is overshadowed, and possibly vibrationally coupled to W=O_t, by the strong symmetric W=O_t vibration. If it is assumed that the symmetric V=O_t vibration also occurs at 1022 cm^{-1}, this results in a V=O_t bond length of 0.1585 nm. The surface VO_x species expelled from the primary Keggin structure give rise to a band at ~1034 cm^{-1} that corresponds to a V=O_t bond length of 0.1579 nm. These W=O_t and V=O_t vibrations and short bond lengths correspond to monooxo tungsten oxide and vanadium oxide molecular structures, resepctively.[35]

In Situ UV−Vis DRS under Dehydrated Conditions. The in situ UV−vis DRS spectra of TPA, TPAV, and the supported VOTPA catalyst samples are presented in Figure 5 plotted as the Kubelka−Munk function using the methods described by Gao[18] and Ross-Medgaarden.[19] The ligand to metal charge transfer (LMCT) transition for the W^{6+} cation appears between 250 and 300 nm, and the LMCT of the V^{+5} cation appears between 350 and 450 nm. Introduction of vanadium into the TPA Keggin introduces a new band between 350 and 450 nm with an E_g value that is ~1 eV lower than that for TPA (see Table 3 for exact values). The E_g values for the TPAV catalyst samples are comparable, and that for the VOTPA Keggin is only slightly lower.

CH_3OH-TPSR Spectroscopy. The CH_3OH-TPSR experiments were conducted to chemically probe the surface chemistry of the TPA, TPAV, and VOTPA catalysts, and the results are presented in Figure 6. It is well-known that methanol chemisorption at 100 °C on oxides forms surface CH_3O* intermediates that dehydrogenate to form H_2CO on surface redox sites and deoxygenate on surface acid sites to form CH_3OCH_3 (DME)

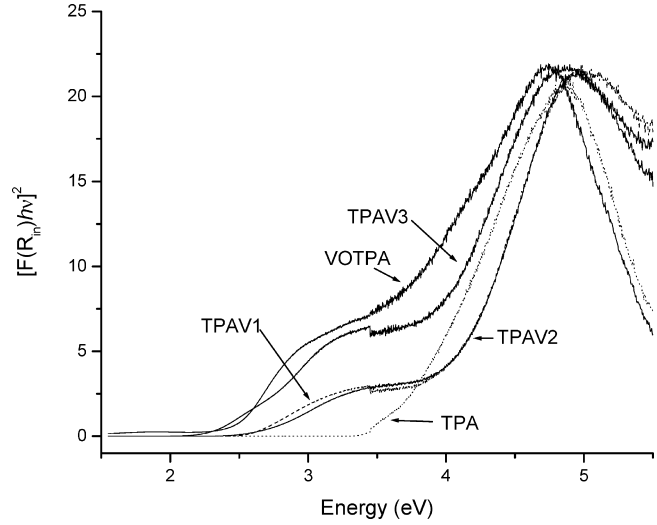

Figure 5. In situ UV−vis spectra of dehydrated TPA and V-containing tungstophosphoric acid catalysts (T = 225 °C).

Table 3. UV−Vis DRS Edge Energy Values (eV) for TPA and the Vanadium-Containing Tungstophosphoric Acid (VOTPA, TPAV1, TPAV2, and TPAV3) Catalysts under Different Environmental Conditions

	edge energy (eV)	
catalyst	dehydrated at 225 °C	in situ during MeOH oxidation at 225 °C
TPA	3.22	3.23
VOTPA	2.05	1.93
TPAV1	2.30	2.25
TPAV2	2.34	2.25
TPAV3	2.28	2.08

from the reaction of surface CH_3* and CH_3O* intermediates.[20,36] The CH_3OH-TPSR spectrum of the vanadium-free TPA Keggin catalyst exclusively yields CH_3OCH_3 with T_p = 182 °C, which reflects the surface Bronsted acid sites present on this POM Keggin.[37] The addition of vanadium oxide to the TPA Keggin does not change the CH_3OCH T_p value, indicating that the same surface Bronsted acid sites are also present for the TPAV Keggins. The incorporation of vanadium oxide into the TPA Keggin structure results in the formation of H_2CO at a $T_p \approx$ 205 °C from the surface redox sites (see Figure 6). The HCHO/DME formation ratio during CH_3OH-TPSR increases linearly from TPAV1 to TPAV3 as indicated in Table 4.

The supported VOTPA catalyst, however, indicates a significantly less active V-containing redox site. The CH_3OH-TPSR spectrum for the supported VOTPA catalyst is also shown in Figure 6 and yields significant amounts of H_2CO with a HCHO/DME formation ratio intermediate between those of TPAV1 and TPAV2. The surface VO_x species on TPA, however, significantly affect the kinetics for breaking the surface methoxy C−H bond by shifting the H_2CO T_p value from 205 to 245 °C. This reveals that the vanadium oxide redox sites incorporated into the primary Keggin structure in the TPAV catalysts are significantly more active than the surface VO_x redox sites present on VOTPA for surface methoxy C−H bond breaking. A closer examination of the H_2CO/CH_3OH-TPSR spectra in Figure 6

(31) Hardcastle, F. D.; Wachs, I. E. *J. Phys. Chem.* **1991**, *95*, 5031.
(32) Gao, X.; Jehng, J.-M.; Wachs, I. E. *J. Catal.* **2002**, *209*, 43.
(33) Scheithauer, M.; Grasselli, R. K.; Knozinger, H. *Langmuir* **1998**, *14*, 3019.
(34) Hardcastle, F. D.; Wachs, I. E. *J. Raman Spectrosc.* **1995**, *26*, 397.
(35) Lee, E. L.; Wachs, I. E. *J. Phys. Chem. C* **2007**, *111*, 4410.
(36) Burcham, L. J.; Briand, L. E.; Waches, I. E. *Langmuir* **2001**, *17*, 617.
(37) Moffat, J. B. *Metal-Oxygen Cluster: The Surface and Catalytic Properties of Heteropolyoxometalates*; Kluwer Academic-Plenum: New York, 2001.

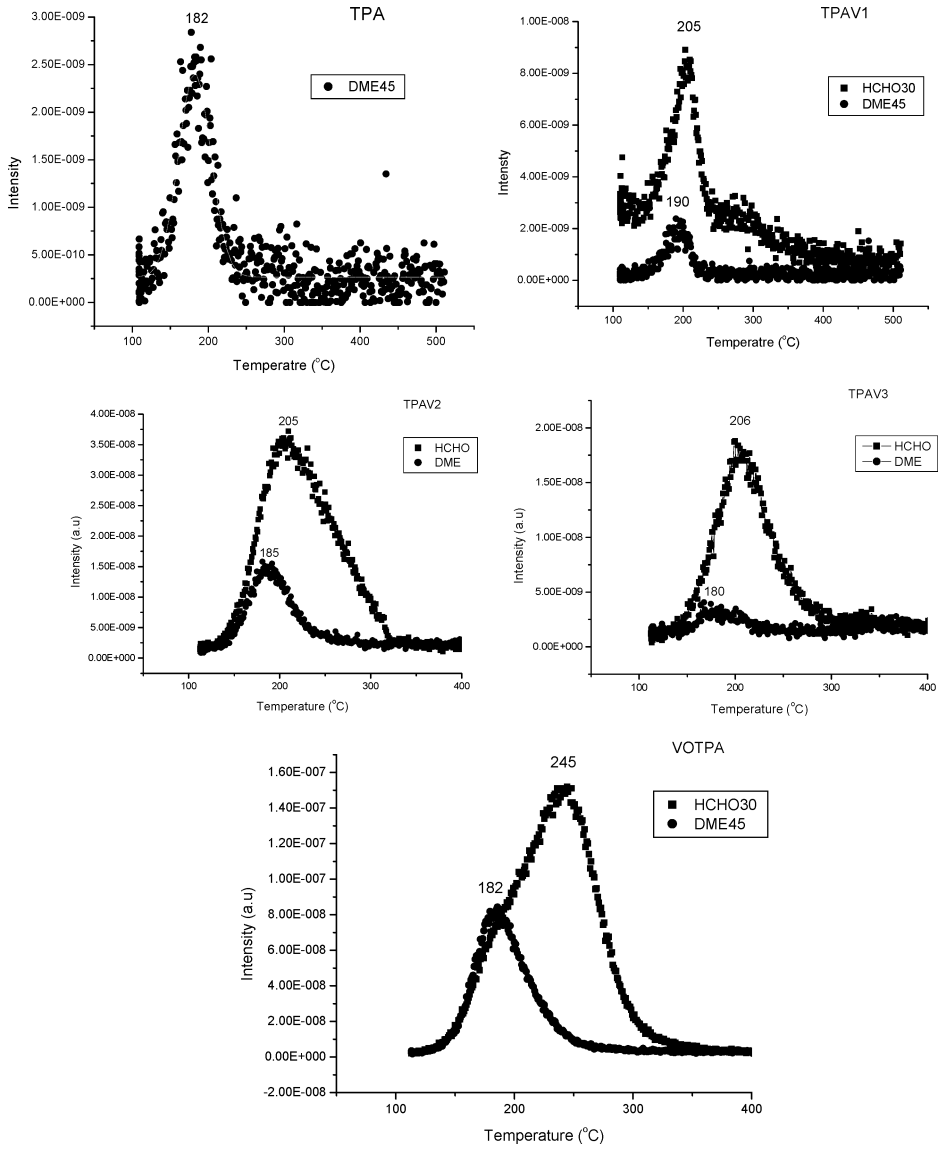

Figure 6. CH_3OH-TPSR spectra for V-containing tungstophosphoric acid catalysts.

Table 4. Relative H_2CO/DME Ratio during CH_3OH-TPSR from the Tungsta-Based Polyoxometallate Catalysts

catalyst	T_p of HCHO (°C)	T_p of DME (°C)	HCHO/DME ratio (arbitrary units)
TPA		182	0.0
TPAV1	205	190	2.1
TPAV2	205	185	4.2
TPAV3	206	180	8.8
VOTPA	245	182	3.1

Table 5. Steady-State Methanol Oxidation Data over the Tungsta-Based Polyoxometallate Catalysts

				selectivity		TOF (s^{-1})	
catalyst	temperature (°C)	conversion (%)	activity (mol/(g of catalyst s))	DME	HCHO	acid	redox
TPA	225	18	9.6	100	0	3.9	0.0
TPAV1	225	22	14.7	82	18	7.6	0.32
TPAV2	225	8	7.4	90	10	0.46	0.010
TPAV3	225	5.6	3.0	100	0	1.9	0.00
VOTPA	250	23	12.5	88	12	0.12	0.0054
VOTPA	225 (extrapolated)					0.046	0.0021

reveals that surface VO_x sites are also present in the TPAV catalysts since they also exhibit a significant H_2CO formation tail in the 245 °C region. The TPAV1 catalyst has only a minor amount of surface VO_x species, but the TPAV2 and TPVA3 catalysts contain appreciable quantities of surface VO_x sites as judged from the trailing tails of the HCHO/CH_3OH-TPSR spectra.

CH_3OH Oxidation/Dehydration. The steady-state methanol oxidation/dehydration reaction over TPA, TPAV, and supported VOTPA catalysts was also examined in the 200−250 °C temperature range where the TPAV catalysts are known to be thermally stable (see the Supporting Information, Figures SI-1−SI-5). The reaction results for TPA and the TPAV catalysts at 225 °C are presented in Table 5. The dominant reaction product from the TPA and TPAV catalysts is DME from the surface acid sites, and H_2CO is the main product from surface redox sites. Small amounts of methyl formate and dimethoxymethane were also formed by secondary reaction of formaldehyde with surface redox and acid sites, and carbon oxide products were not observed. The redox selectivity, TOF values, and TOF_{redox}/TOF_{acid} ratio do not monotonically increase with increasing vanadium content of the TPA. The TPAV3 catalyst with the highest vanadium content does not even form HCHO

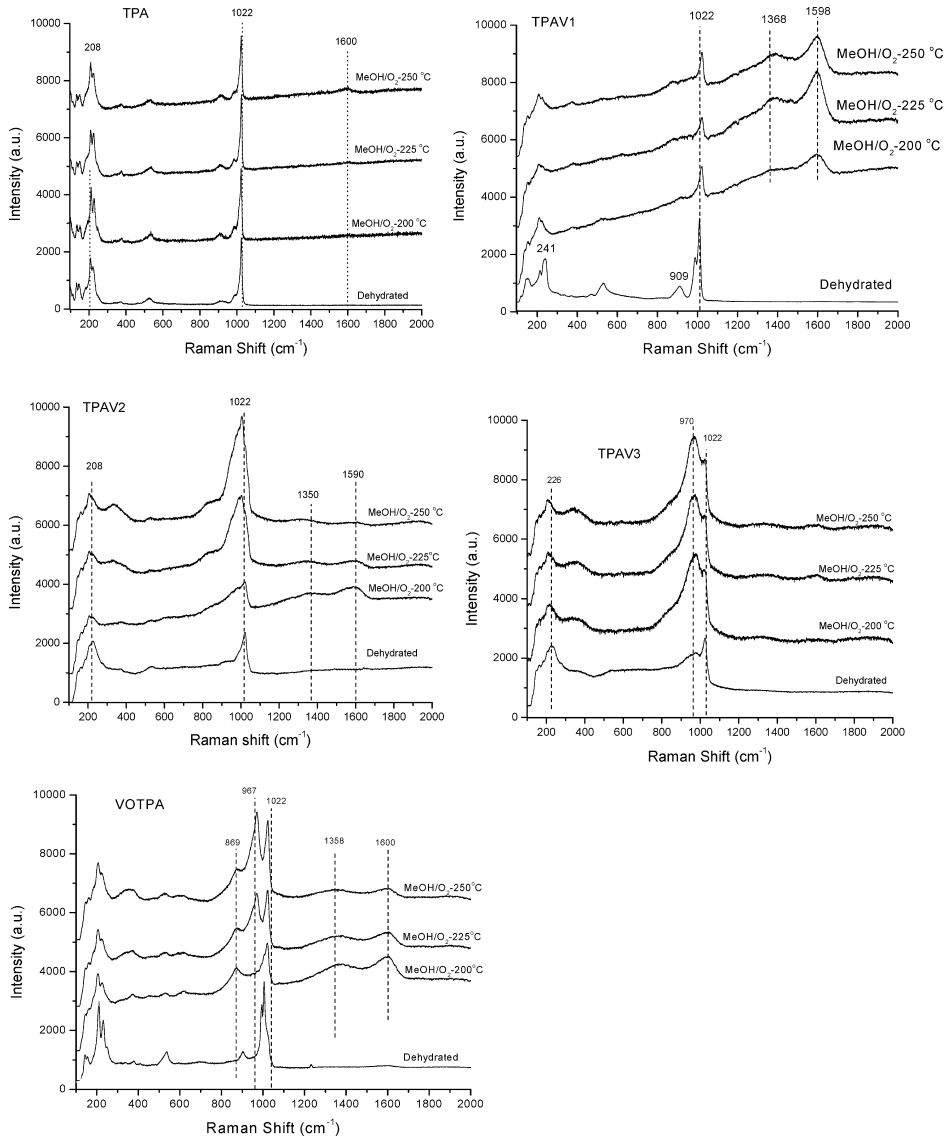

Figure 7. In situ Raman spectra of vanadium-containing tungstophosphoric acid catalysts during methanol oxidation/dehydration reaction conditions (T = 225 °C, O_2/CH_3OH = 2.17). The Keggin W−O−W bending modes at ∼220−250 cm^{-1} are employed as the internal standard.

during steady-state reaction, and DME is the only reaction product. The TOF values are highest for the TPAV1 catalyst and decrease with increasing vanadia content for both the surface redox and acid sites, especially for the TOF_{redox} kinetics. Similar activity and selectivity trends have also been found for vanadium-containing molybdenum POMs (MPAs).[9,38,39]

The supported VOTPA catalyst was found to be barely active for methanol oxidation at 225 °C, requiring reaction studies at 250 °C for appreciable methanol conversion (see Table 5). The TOF for supported VOTPA was experimentally determined at 250 °C and extrapolated to 225 °C, which is also reported in Table 5. The significantly lower catalytic activity of the supported VOTPA catalyst further confirms that surface VO_x sites in the secondary structure of the TPA Keggin are significantly less active than the VO_x sites incorporated into the primary Keggin structure and is consistent with the HCHO/CH_3OH-TPSR studies reported above. Thus, at the reaction temperature of 225 °C the surface VO_x species in the secondary structure are essentially poisons that shut off catalytic activity.

In Situ Raman Spectroscopy during CH_3OH Oxidation/Dehydration. To better understand the state of these V-containing TPA-based catalysts during steady-state CH_3OH oxidation, in situ Raman spectroscopy studies were conducted under the methanol oxidation/dehydration reaction conditions. The in situ Raman spectra of the TPA, TPAV, and supported VOTPA catalysts during methanol oxidation/dehydration as a function of reaction temperature in the 200−250 °C range, where the TPA, TPAV, and supported VOTPA catalyst samples are thermally stable (see the Supporting Information, Figures SI-1−SI-5), are presented in Figure 7. The Raman spectrum for the TPAV1 catalyst exhibits new bands at ∼1350 and ∼1600 cm^{-1} as well as the characteristic bands of the Keggin TPA structure under methanol oxidation/dehydration conditions. The new Raman bands at ∼1350 and ∼1600 cm^{-1} correspond to polyaromatic coke and reveal that carbon deposition on the TPA catalyst is taking place during methanol oxidation.[40] The amount of carbon deposited on the TPAV catalyst decreases with increasing content of vanadium as shown for TPAV1, TPAV2, and TPAV3, and there is almost no coke present for TPAV3 during methanol oxidation. The amount of surface carbon further

(38) Liu, H.; Iglesia, E. *J. Phy. Chem. B* **2003**, *107*, 10840.
(39) Liu, H.; Iglesia, E. *J. Catal.* **2004**, *223*, 161.

decreases with increasing reaction temperature. Surprisingly, only a small amount of carbon is deposited on the acidic TPA catalyst. The VOTPA catalyst exhibits modest amounts of carbon deposition and is almost free of coke at 250 °C.

The corresponding in situ Raman bands from the Keggin unit provide structural information about the TPA Keggins under the methanol oxidation reaction conditions (200−250 °C). The characteristic Keggin Raman bands are present under reaction conditions for TPA, TPAV1, and TPAV2 catalysts and reflect the structural integrity of the Keggin unit for these mixed metal oxide catalysts during methanol oxidation in this temperature range. The TPAV2 catalyst, however, also exhibits a broad shoulder on the low-wavenumber side of the major W=O_t vibrational band. Further increasing the vanadium content to TPAV3 significantly broadens the Keggin vibration at 1022 cm^{-1} and also reveals the formation of a new broad band at ~970 cm^{-1}. The weakening and broadening of the primary Keggin vibrations for TPAV2 and TPAV3 reflects the structural disorder introduced by the presence of increasing amounts of vanadium in the primary Keggin unit. Such structural disorder of the primary Keggin unit is not observed for the TPAV1 and VOTPA catalysts where vanadium oxide has been substituted into the Keggin unit and is present as surface VO_x species, respectively.

The presence of the surface VO_x species on the TPA support in supported VOTPA, however, gives rise to additional sharp Raman bands at ~970 and 870 cm^{-1} during methanol oxidation at elevated temperatures. These vibrational bands have been shown above to occur when surface VO_x species perturb the asymmetric vibrations of the W=O_t and W−O_b−W functionalities. The shift of the W=O_t vibration from 1022 to 970 cm^{-1} is related to perturbation of the vibrational coupling of adjacent W=O_t bonds. The enhanced 870 cm^{-1} band is probably related to perturbation of the W−O_b−W vibration by the surface VO_x species and/or surface methoxy species. The presence of the ~970 cm^{-1} band in the Raman spectra of TPAV2 and TPAV3 also reflects the presence of surface VO_x species in the secondary structure of the Keggin units in these samples. The enhanced perturbations of the TPA Keggin W=O_t and W−O_b−W vibrations during methanol oxidation reveal that the surface VO_x species are well dispersed on the TPA and TPAV supports. These in situ Raman findings are in agreement with the above CH_3OH-TPSR spectra (see Figure 6 and discussion above), indicating that surface VO_x species are present on the outer surface or secondary structure of the TPAV Keggin units, especially for TPAV2 and TPAV3.

In Situ UV−Vis DRS during Methanol Oxidation/Dehydration. The in situ UV−vis spectra were also obtained during methanol oxidation/dehydration at 225 °C (see the Supporting Information, Figures SI-6−SI-9). There is an indication of only a minor reduction in the V^{5+} LMCT and a slight increase in the V^{3+}/V^{4+} d−d transition region, most probably related to the small carbon deposition that also gives rise to a UV−vis signal in this region, indicating that the vanadium oxide sites in the TPA Keggin are primarily present as V^{5+} during methanol oxidation/dehydration at 225 °C (O_2/CH_3OH = 2.17). This behavior is consistent with the Mars−van Krevelen mechanism and the rapid reoxidation kinetics of the vanadia sites by gas-phase molecular O_2.

Discussion

Bulk or Primary Keggin Structures. The $H_{3+x}PW_{12-x}V_xO_{40}$ Keggins retain the primary TPA structure upon incorporation of vanadium oxide. Broadening of the Raman bands indicates that the incorporated vanadium oxide is creating structural disorder in the primary Keggin structure, most likely by occupying different primary sites. Solid-state MAS ^{51}V NMR confirms that the incorporated vanadia possess VO_6 coordination, which reflects substitution of VO_6 for WO_6 in the TPA Keggin structure. UV−vis DRS reveals that the Keggin E_g value decreases by ~1 eV by incorporation of vanadia into the TPA Keggin. When the E_g values for the dehydrated TPAV and VOTPA Keggins are evaluated using the V−O−V correlation ($N = 14.03 - 3.95E_g$),[18] the correlation indicates that four bridging V−O−V bonds are present for every V-containing TPA Keggin. However, the V-containing TPA Keggins mostly contain V−O−W and not V−O−V bonds because of the minority concentration of vanadium oxide. This indicates that the correlation published by Gao et al.[18] also holds up when the vanadium cation is bonded to other metal oxide cations such as tungsten oxide.

Dehydration of the Keggins results in removal of crystal water and shifting of the W=O_t vibrations from 1011 to 1022 cm^{-1}. Similar shifts in the infrared spectra of W=O_t bonds of $H_3PW_{12}O_{40}$ upon dehydration were previously proposed to result from proton movement from the terminal W=O_t bond to the bridging W−O−W bond,[41] but such changes in the W=O_t vibrations are routinely observed for supported tungsten oxide catalysts and just reflect the removal of hydrogen-bonded water from the W=O_t bond upon dehydration.[42,43] The Raman bands of the dehydrated V-containing Keggins are also broadened relative to those of TPA due to structural disorder, and the broadening increases with increasing vanadium content. The addition of vanadium oxide to the TPA Keggin results in thermal decomposition of the $H_{3+x}PW_{12-x}V_xO_{40}$ Keggins in the 400−500 °C range, with greater instability paralleling increasing vanadium oxide content. The origin of this thermal instability is most probability related to the much lower Tammann temperature of vanadium oxide (~200 °C) compared to tungsten oxide (~600 °C), which is responsible for the enhanced mobility of vanadium oxide. Decomposition of the V-containing TPA Keggins is accompanied by expulsion of VO_x, exhibiting a V=O_t vibration at ~1034 cm^{-1}, and formation of poorly ordered WO_3 NPs (Raman vibrations at ~690 and ~790 cm^{-1}).

During methanol oxidation/dehydration the in situ Raman bands of the primary Keggins further broaden with vanadium oxide content relative to those of the dehydrated catalysts. This may be related to the enhanced mobility of vanadium oxide by formation of mobile surface V−OCH_3 complexes[44] and the coordination of surface methoxy species. The corresponding in situ UV−vis DRS spectra show that the vanadium oxide sites remain essentially fully oxidized during methanol oxidation/dehydration at 250 °C. Thus, the primary structures of the

(40) Li, C.; Stair, P. C. *Catal. Today* **1997**, *33*, 353.
(41) Lee, K. Y.; Mizuno, N.; Okuhara, T.; Misono, M. *Bull. Chem. Soc. Jpn.* **1989**, *62*, 1731.
(42) Kim, D. S.; Ostromecki, M.; Wachs, I. E. *J. Mol. Catal. A* **1996**, *106*, 93.
(43) Kim, T.; Burrows, A.; Kiely, C. J.; Wachs, I. E. *J. Mol. Catal.* **2007**, *246*, 370.
(44) Wang, C.-B.; Cai, Y.; Wachs, I. E. *Langmuir* **1999**, *15*, 1223.

V-containing TPA Keggins remain intact during methanol oxidation, but are structurally disordered by the introduction of vanadium oxide and the reaction conditions.

The VO_x sites essentially remain fully oxidized during the methanol oxidation/dehydration reactions with an O_2/CH_3OH ratio of 2.17 (see the Supporting Information, Figures SI-6−SI-9). This indicates that the methanol oxidation kinetics follows a Mars−van Krevelen mechanism where the reduced vanadium oxide sites are rapidly reoxidized by gas-phase molecular O_2.

Surface or Secondary Keggin Structures. The V-containing TPA Keggins also possess significant surface VO_x sites in their initial synthesized state, which are distinct from expelled surface VO_x species on defective Keggins (Raman band at $\sim$1034 cm^{-1}) observed at elevated temperatures (see the Supporting Information, Figures SI-2−SI-4). The presence of surface VO_x species in the supported VOTPA Keggin perturbs the vibrational coupling of adjacent $W{=}O_t$ bonds and shifts the symmetric $W{=}O_t$ vibration toward 970 cm^{-1}. The $W-O_b-W$ vibration at $\sim$870 cm^{-1} is also perturbed by the surface VO_x and methoxy species. These vibrations have previously been assigned to defective Keggin structures,[41] but the current study has shown that expulsion of VO_x from the TPAV Keggins is not accompanied by enhanced Raman bands at $\sim$970−990 and $\sim$870 cm^{-1} (see the Supporting Information, Figures SI-2−SI-4). It, thus, appears that the surface VO_x species are perturbing the symmetric $W{=}O_t$ vibration. These perturbations by the surface VO_x species are further enhanced during methanol oxidation and may be related to the greater mobility of surface $V-OCH_3$ complexes and the presence of surface $W-OCH_3$ species (see Figure 7).

Polyaromatic carbon deposition on the surface of the TPAV Keggins also takes place during steady-state methanol oxidation (see Raman bands at $\sim$1360 and $\sim$1600 cm^{-1} in Figure 7).[40] The extent of carbon deposition is related to the amount of vanadium oxide in the TPAV Keggin since the V-free TPA exhibits a negligible amount of carbon deposition and the amount of surface carbon decreases with vanadium content (TPAV1 > TPAV2 > TPAV3). Thus, the vanadium oxide sites appear to be involved in both the carbon formation and carbon combustion reactions. The amount of surface carbon present during steady-state methanol oxidation at 225 °C, however, must be minimal since the UV−vis DRS background in the 400−800 nm region was not significantly perturbed by the deposited carbon at the reaction temperature of 225 °C (see the Supporting Information, Figures SI-6−SI-9).[45]

Surface Chemistry. The surface acid sites present in the $H_3PW_{12}O_{40}$ Keggin are extremely active for breaking the surface methoxy C−O bond involved in the formation of CH_3OCH_3 compared to surface acid sites present on other tungsten oxide-based catalysts. The DME/CH_3OH-TPSR of $T_p \approx 180$ °C reflects much faster surface kinetics than found for unsupported WO_3 ($T_p \approx 260$ °C),[46,47] supported WO_3/ZrO_2 with monolayer surface WO_x coverage ($T_p \approx 290$ °C),[47] and even the highly acidic WO_3-ZrO_2 catalyst ($T_p \approx 216$ °C) produced by reacting ammonium metatungstate with $ZrO(OH)_2$.[48,49] The supported WO_3/Al_2O_3 catalyst system ($T_p \approx 206$ °C), however, is slightly more active than the other supported WO_3 catalysts, but is still less active than the $H_3PW_{12}O_{40}$ Keggin ($T_p \approx 180$ °C).

The surface redox sites in the TPAV Keggins break the surface methoxy C−H bond at $\sim$205 °C. This is consistent with corresponding CH_3OH-TPSR results for bulk V_2O_5 ($T_p = 200$ °C)[46] and supported V_2O_5 catalysts ($T_p \approx 180-190$ °C),[30,49] which indicates comparable redox kinetics for breaking the surface methoxy C−H bond for the V-containing TPA Keggins, bulk V_2O_5, and supported vanadium oxide catalysts. The surface VO_x species present in the secondary Keggin structure of supported VOTPA catalysts, however, exhibit a $T_p \approx 245$ °C, indicating much lower redox activity of the surface VO_x species compared to the VO_x sites incorporated in the primary TPA Keggin structure.

Structure−Catalytic Activity Relationships. There are two distinct VO_x redox sites in the TPAV catalysts: VO_x sites in the primary TPA Keggin structure and VO_x sites on the surface or secondary TPA Keggin structure (see the above discussion in the "Surface or Secondary Keggin Structures" section). The steady-state methanol oxidation to formaldehyde studies at 225 °C revealed that VO_x sites in the primary Keggin structure exhibit a TOF that is $\sim$160 times greater than that of the surface VO_x sites. The continuous decrease in TOF_{redox} in going from TPAV1 to TPAV2 to TPAV3 reflects the increasing concentration of surface VO_x sites in the secondary structure of the Keggins with increasing vanadium oxide content. The catalytic poisoning effect of surface VO_x species in the secondary structure of V-containing Keggin catalysts was not previously fully appreciated in the literature.[9,10,38,39]

The minor amount of surface carbon deposition may also affect the catalytic activity, and the amount of surface carbon decreases with vanadium oxide content, which follows the opposite of the activity trend, and its quantitative effect on the TOF_{redox} is not known. The contribution of the surface carbon to the methanol oxidation kinetics over the $H_{3+x}PW_{12-x}V_xO_{40}$ Keggins, however, can be neglected in a first approximation because of the inverse relationship between TOF_{redox} and vanadium oxide content and its minor amounts.

Comparison of the TOF_{redox} kinetics with the UV−vis DRS E_g values reveals that a relationship between the electronic structure and TOF_{redox} kinetics for the $H_{3+x}PW_{12-x}V_xO_{40}$ Keggins does not exist. Although the addition of vanadium oxide to the TPA Keggins introduces redox sites and lowers the E_g value, which reflects enhanced electron delocalization, there is no correlation with the TOF_{redox} kinetics. The UV−vis E_g values for the TPAV1, TPAV2, and TPAV3 Keggins are comparable, but their corresponding TOF_{redox} kinetics decrease by orders of magnitude. The supported VOTPA catalyst possesses a lower E_g value than the TPAV catalysts and is even less active for methanol oxidation to formaldehyde, which is the opposite of what would be anticipated for its lower E_g value and greater electron delocalization. The current UV−vis DRS and steady-state methanol oxidation kinetics demonstrate that correlations between E_g and TOF_{redox} for Keggins should be carefully viewed.

Comparison of the methanol oxidation to formaldehyde reaction rates for the $H_{3+x}PW_{12-x}V_xO_{40}$ and supported $VO_x/H_3PW_{12}O_{40}$ Keggins with unsupported V_2O_5 and supported V_2O_5 catalysts provides interesting insights into the catalytic activity of these V-containing Keggin catalysts. The steady-state methanol oxidation specific reaction rate for TPAV1 ($TOF_{redox} = 0.3$ s^{-1} at 225 °C) is comparable to that found for bulk V_2O_5

(45) Tinnemans, S. J.; Kox, M. H. F.; Sletering, M. W.; Nijhuis, T. A.; Visser, T.; Weckhuysen, B. M. *Phys. Chem. Chem. Phys.* **2006**, *8*, 2413.
(46) Badlani, M.; Wachs, I. E. *Catal. Lett.* **2001**, *75*, 1.
(47) Kim, T.; Wachs, I. E. *J. Catal.* **2007**, *246*, 370.
(48) Ross-Medgaarden,; Knowles, W. V.; Kim, T.; Wong, M. S.; Zhou, W.; Kiely, C. J.; Wachs, I. E. *J. Catal.* **2008**, *256*, 108.
(49) Kim, T. Ph.D. Thesis, Lehigh University, 2007.

(TOF_{redox} = 1.1 s^{-1} at 230 °C),[46] supported V_2O_5/CeO_2 (TOF_{redox} = 1.0 s^{-1} at 230 °C),[50] supported V_2O_5/ZrO_2 (TOF_{redox} = 0.17 s^{-1} at 230 °C),[50] and supported V_2O_5/TiO_2 (TOF_{redox} = 0.11 s^{-1} at 230 °C).[50] The TPAV1 TOF_{redox} value, however, is much greater than found for the supported V_2O_5/Al_2O_3 (TOF_{redox} = 0.007 s^{-1} at 230 °C)[48−50] and supported V_2O_5/SiO_2 (TOF_{redox} = 0.002 s^{-1} at 230 °C) catalysts.[50] Thus, the specific reaction rate for TPAV1, which contains minimal amounts of surface VO_x species in the secondary structure of the $H_{3+x}PW_{12-x}V_xO_{40}$ Keggin, is comparable to the most active V-containing catalysts. The surface VO_x species in the secondary structure of the $H_{3+x}PW_{12-x}V_xO_{40}$ Keggin and coordinated to the Keggin WO_x sites, however, possess an extremely low specific redox activity (TOF = 0.002 at 225 °C) that is comparable to that of the least active supported V_2O_5/SiO_2 catalyst (TOF_{redox} = 0.007 at 230 °C).

Comparison of the steady-state methanol dehydration kinetics by the $H_{3+x}PW_{12-x}V_xO_{40}$ Keggins with those for bulk WO_3 and supported WO_3 catalysts provides additional insights into the catalytic acidic properties of the W-containing Keggins. The dehydration kinetics by the $H_3PW_{12}O_{40}$ Keggin (TOF_{acid} = 3.9 s^{-1} at 225 °C) is significantly faster than that for bulk WO_3 (TOF_{acid} = 0.03 s^{-1} at 230 °C)[47,49] and the supported WO_3 catalysts ($TOF_{acid} \approx 0.02-0.08$ s^{-1} at 230 °C for WO_3/ZrO_2, WO_3/TiO_2, WO_3/Nb_2O_5, and WO_3/Al_2O_3).[47] The methanol dehydration TOF_{acid} for $H_3PWo_{12}O_{40}$ is even 2 orders of magnitude faster than that found for the highly active ZrO_x-stabilized WO_3 nanoparticles present in the coprecipitated WO_3-ZrO_2 catalysts (TOF_{acid} = 0.05 s^{-1} at 225 °C).[48] Thus, the surface acid sites present in the $H_3PWo_{12}O_{40}$ Keggin are highly acidic for methanol dehydration, and their kinetics are significantly faster than those of other W-containing catalysts (bulk WO_3, supported WO_3 catalysts, and even the highly acidic WO_3-ZrO_2 catalyst synthesized by AMT and $ZrO(OH)_2$ coprecipitation). The steady-state methanol dehydration TOF_{acid} values track the large variation in the DME/CH_3OH-TPSR trends reported above (180 °C < T_p < 290 °C), which suggests that breaking of the surface methoxy C−O bond dominates the steady-state catalytic activity trend.

Introduction of VO_x sites into the $H_3PW_{12}O_{40}$ Keggin also modifies its acidic character. Surface VO_x sites on TPA decrease the TOF_{acid} kinetics by ~100-fold from site blocking and titration of acidic surface hydroxyls. Incorporation of VO_x into the TPA Keggin does not affect the TOF_{acid} kinetics for TPAV1, which has only a minimal amount of surface VO_x sites. The TOF_{acid} kinetics for TPAV2 and TPAV3, however, are lower than that for TPAV1 because of the greater presence of surface VO_x sites. As for the methanol oxidation TOF_{redox} kinetics, the methanol dehydration TOF_{acid} kinetics over the Keggins do not correlate with the UV−vis E_g value, as well as the amount of carbon deposition, since the TOF_{acid} values are essentially the same for TPA and TPAV1.

Conclusions

The $H_{3+x}PW_{12-x}VxO_{40}$ Keggins contain VO_x sites in both the primary and secondary structures. The vanadium oxide incorporated into the primary structure possesses VO_6 coordination and has substituted for WO_6 units in the Keggin. The vanadium oxide in the secondary structures possesses the same structure under ambient conditions. Introduction of the VO_x units into the primary $H_{3+x}PW_{12-x}V_xO_{40}$ Keggin structure causes structural disorder and lowers the thermal stability of the Keggin clusters, which is much less pronounced for the surface VO_x species or vanadium oxide in the secondary structure.

The structurally disordered $H_{3+x}PW_{12-x}VxO_{40}$ clusters remain intact during methanol oxidation/dehydration in the 200−250 °C range. The VO_x units in the primary and secondary structures are essentially fully oxidized as V^{5+} during the methanol oxidation/dehydration reaction (O_2/CH_3OH = 2.17), which reflects the operation of the Mars−van Krevelen redox mechanism and the rapid reoxidation by gas-phase molecular O_2. The vanadium oxide site in the primary Keggin structure is ~160 times more active for methanol oxidation to formaldehyde at 225 °C than the vanadium oxide site in the secondary structure. The decreasing TOF_{redox} kinetics with increasing vanadium oxide content in the $H_{3+x}PW_{12-x}V_xO_{40}$ Keggins is a consequence of the increasing amount of vanadium oxide in the Keggin secondary structure as the V content is increased. The presence of the surface VO_x species on the Keggin cluster also retards the TOF_{acid} kinetics for methanol dehydration because the surface VO_x species block access to WO_x acid sites and titrate acidic surface hydroxyls.

The methanol dehydration kinetics (TOF_{acid}) over the $H_3PW_{12}O_{40}$ Keggin is ~100 times faster than for bulk WO_3 and supported tungsten oxide catalysts, which reflects the strong acidic character of the protons in the TPA Keggin cluster. The presence of surface VO_x species can reduce the TOF_{acid} kinetics by as much as a factor of ~100. The methanol oxidation to formaldehyde kinetics (TOF_{redox}) over $H_4PW_{11}V_1O_{40}$ is comparable to that for the more active vanadium oxide catalysts (bulk V_2O_5 and supported V_2O_5/CeO_2, V_2O_5/ZrO_2, and V_2O_5/TiO_2). The TOF_{redox} kinetics for the supported $VO_x/H_3PW_{12}O_{40}$ Keggin catalyst is comparable to that of the least active supported vanadium oxide catalyst (V_2O_5/SiO_2).

No correlations were found between the electronic E_g values and the methanol oxidation TOF_{redox} and methanol dehydration TOF_{acid} kinetics of the $H_{3+x}PW_{12-x}V_xO_{40}$ Keggins. A minor amount of surface carbon is also present on the Keggins during methanol oxidation/dehydration, which decreases with increasing vanadium oxide content, and does not appear to affect the kinetics. These new insights reveal that mixed metal oxide Keggins are much more complex than originally thought and that care must be taken in employing Keggins as model mixed metal oxide NPs in kinetic and theoretical studies.

Acknowledgment. L.N. thanks the Department of Science & Technology, New Delhi, India, for financial assistance in the form of a BOYSCAST fellowship. We thank Prof. Mark A. Barteau, Department of Chemical Engineering, University of Delaware, for providing some of the Keggin catalyst samples. The Lehigh University researchers were supported by NSF Nanoscale Integrated Research Team (NIRT) Grant 0609018.

Supporting Information Available: Information related to the in situ Raman spectra of the catalysts obtained at different temperatures and the in situ UV−vis DRS carried out under the reaction conditions. This material is available free of charge via the Internet at http://pubs.acs.org/.

JA904957D

(50) Wachs, I. E.; Chen, Y.; Jehng, J.-M.; Briand, L. E.; Tanaka, T. *Catal. Today* **2003**, *78*, 13.